

# Fabric-substrated capacitive biopotential sensors enhanced by dielectric nanoparticles

Xiangjun Chen<sup>1,§</sup>, Xiaoxiang Gao<sup>2,§</sup>, Akihiro Nomoto<sup>2,§</sup>, Keren Shi<sup>1</sup>, Muyang Lin<sup>2</sup>, Hongjie Hu<sup>1</sup>, Yue Gu<sup>1</sup>, Yangzhi Zhu<sup>2</sup>, Zhuohong Wu<sup>2</sup>, Xue Chen<sup>1</sup>, Xinyu Wang<sup>2</sup>, Baiyan Qi<sup>1</sup>, Sai Zhou<sup>1</sup>, Hong Ding<sup>2</sup>, and Sheng Xu<sup>1,2,3,4</sup> (✉)

<sup>1</sup> Materials Science and Engineering Program, University of California San Diego, La Jolla, CA 92093, USA

<sup>2</sup> Department of NanoEngineering, University of California San Diego, La Jolla, CA 92093, USA

<sup>3</sup> Department of Electrical and Computer Engineering, University of California San Diego, La Jolla, CA 92093, USA

<sup>4</sup> Department of Bioengineering, University of California San Diego, La Jolla, CA 92093, USA

<sup>§</sup> Xiangjun Chen, Xiaoxiang Gao, and Akihiro Nomoto contributed equally to this work.

© Tsinghua University Press and Springer-Verlag GmbH Germany, part of Springer Nature 2021

**Received:** 6 January 2021 / **Revised:** 17 March 2021 / **Accepted:** 21 March 2021

## ABSTRACT

Wearable biopotential sensing devices are essential to long-term and real-time monitoring of human health. Non-contact, capacitive sensing electrodes prevent potential skin irritations, and are thus beneficial for long-term monitoring. Existing capacitive electrodes are either connected to a separate control circuit via external wires or have limited sensing capacitances, which leads to low signal qualities. This study demonstrates a stretchable capacitive sensing device with integrated electrodes and control electronics, with enhanced signal qualities. The electrodes and the control electronics are fabricated on a common fabric substrate for breathability and strain-limiting protection. The stretchable electrodes are based on an island-bridge design with a stretchability as high as ~ 100%, and an area ratio as high as ~ 80%. By using a dielectric calcium copper titanate (CCTO) composite as the adhesive layer, the electrode capacitance can be increased, yielding an enhanced signal-to-noise ratio (SNR) in the acquired biopotentials. This device offers a convenient and comfortable approach for long-term non-contact monitoring of biopotential signals.

## KEYWORDS

capacitive sensing, biopotential, stretchable, calcium copper titanate (CCTO), signal-to-noise ratio (SNR)

## 1 Introduction

Biopotential sensing from the skin surface has proved to be valuable for health monitoring [1], diagnostics [2, 3], and human-machine interface [4–6]. In these cases, long-term recording is critical for capturing intermittent or transient events to inform appropriate treatment or predict an adverse event [7, 8]. Wearable biopotential sensors for electrocardiogram (ECG) [9] and electromyogram (EMG) [10] allow for ambulatory data collection over extended periods. Electrodes of wearable sensors in direct contact with the skin may cause skin irritation or inflammation for users who are sensitive to adhesives [11, 12]. Non-contact electrodes that capacitively couple the biopotentials can circumvent this problem [13–18]. Those devices typically use rigid substrates, which do not conform to the soft and curvilinear human body surface, limiting their applications in continuous long-term monitoring. To overcome this challenge, conformal capacitive biopotential monitoring sensors using conductive fabric [19] or filamentary serpentine mesh electrodes on silicone rubber [20, 21] have been demonstrated, but they each have limitations. The challenge with conductive fabrics is that it is difficult to integrate circuits with them, and therefore there are only passive electrodes [22]. The problem with filamentary serpentine mesh electrodes is that they have a relatively small effective area in electrode space that leads to low coupling capacitance and thus compromised signal

quality [20]. Compared to commercial wet conductive electrodes, these electrodes have lower SNR due to low input capacitance and thus high input impedance.

Here we present a stretchable capacitive sensor on a fabric substrate for non-contact monitoring of biopotentials. The electrodes show high stretchability that enables conformal contact with the skin and a large effective area of the electrode that provides high quality of capacitive coupling with skin. Electrodes and the circuit are integrated on the fabric substrate for acquiring and processing of ECG and EMG signals. Due to the porous and fibrous characteristics, the fabric substrate possesses high breathability, which is an excellent candidate serving as the substrate for wearable devices [23–25]. The silicone encapsulation layer is not breathable [26, 27], but the airflow can transport horizontally along the textile substrate. Additionally, we dope an adhesive layer between the electrode and fabric with calcium copper titanate (CCTO) nanoparticles to increase the capacitance and enhance the signal-to-noise ratio (SNR) of the biopotential signal.

## 2 Result and discussion

### 2.1 Characterization of the device

Figure 1(a) depicts the schematics of the device. The device, encapsulated by a 200 μm layer silicone elastomer (modulus

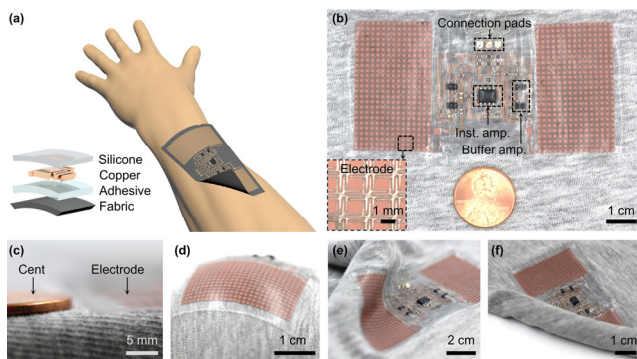


**Figure 1** The schematic and optical images of the stretchable capacitive sensor on a fabric substrate. (a) Illustration of the device on the arm. Inset is an exploded view of the capacitive electrode. (b) An overview of the capacitive sensor. Inset shows magnified view of the electrode. The device consists of four major parts: an instrumentation amplifier (inst. amp.), two sets of buffer amplifiers (buffer amp.), connection pads, and two electrodes. (c) Side view of the capacitive electrode on a fabric. Images of a device in (d) a conformal configuration on a spherical surface, (e) a bloused configuration, and (f) a rolled configuration to show the fabric at the backside of the device.

of  $\sim 60$  kPa, Ecoflex 00–30, Smooth-on), is attached to a  $220 \mu\text{m}$  thick fabric substrate with an adhesive layer (modulus of  $\sim 3$  kPa, Silbione RT Gel 4717 A/B, Bluestar Silicones), which provides breathability and physical support. There is no direct contact between the skin and the device. The device is composed of a central integrated circuit hub and two side electrodes. A schematic exploded-view reveals the layered structure of the electrode, where a  $20 \mu\text{m}$  copper layer with an island-bridge structure couples with biopotentials capacitively. At the central circuit hub, integrated circuit chips are bonded on the copper electrodes in island-bridge layouts. The central circuit hub includes instrumentation amplifiers, buffer amplifiers, and necessary passive components (see Fig. S1 in the Electronic Supplementary Material (ESM) for more details of the circuit).

## 2.2 Design and stretchability of the electrode

The key for capacitive electrode design is to maximize the area filling ratio and therefore the capacitance. Figure 2(a) portrays the capacitive electrode layout, which is composed of square islands and serpentine bridges. The parameters of design include island size  $I$ , bridge wire width  $L$ , and inter-bridge spacing  $S$ . Considering the spatial resolution of the patterning technique for the copper electrode is  $40 \mu\text{m}$  [28], to ensure the fabrication yield, in this work we use  $L$  and  $S$  of  $150$  and  $50 \mu\text{m}$ , respectively. Figure 2(b) shows the calculated area filling ratio of the electrode as a function of the island size  $I$ . For capacitive sensing, both islands and bridges of the electrodes will couple biopotentials and should therefore be considered in the optimization. The island-bridge design has an area filling ratio of  $80\%$  where island size is  $1$  mm, much higher than the bridge-only design where island size is close to  $0 \mu\text{m}$ , demonstrating the advantage of this design compared with the filamentary serpentine mesh electrode [20].

The optimal island size is determined by the stretchability of the electrode. A larger island size leads to lower stretchability. Uniaxial stretching test results show no delamination at  $100\%$  tensile strain with an island size from  $0.5$  to  $2$  mm, while maintaining a high area ratio (Fig. S2 in the ESM). In addition, stress-strain testing of the electrode integrated on the fabric shows similar results to the bare fabric, which indicates the minimal mechanical load of the electrode imposed on the fabric (Fig. 2(c)). The fabric breaks at  $100\%$  tensile strain, before

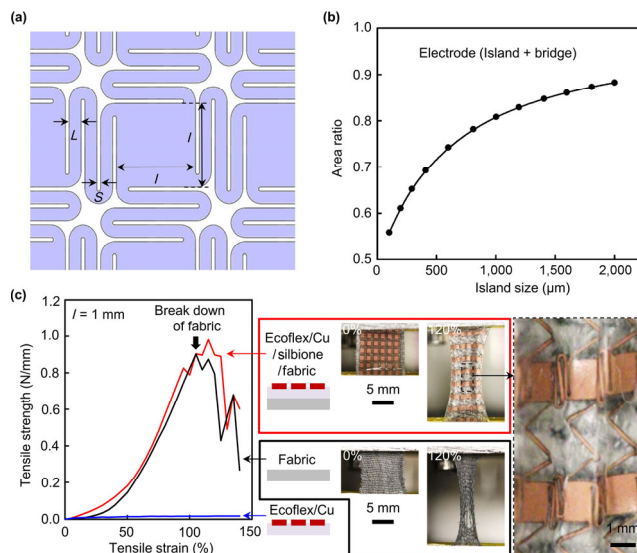


**Figure 2** Geometric design and stretchability characterization of the electrode. (a) Detailed structure of one electrode island. Key geometric parameters include the island size  $I$ , bridge wire width  $L$ , and the gap width between bridges  $S$ . (b) The relationship between the area ratio and island width. (c) Stretchability tests of the standalone electrode, the bare fabric substrate, and the electrode integrated on the fabric. The copper electrode integrated on the fabric substrate shows a stress-strain behavior similar to the bare fabric substrate, illustrating the minimal mechanical load imposed by the stretchable electrode.

the copper electrode breaks, so the fabric can function as a strain-limiting protection for the electrode [29].

## 2.3 Electrical properties of the electrode

To test if any mechanical deformation will influence the performance of the electrodes, we characterized the capacitance of the electrodes under tensile strain. Figures 3(a) and 3(b) show a photo and schematic illustration of the experimental setup. We gradually stretch the electrode while monitoring the capacitance change using a digital multimeter (A.W. SPERRY DM-8500). Due to Poisson's ratio, the tensile strain decreases the thickness of the fabric layer, thus increasing the capacitance (Fig. 3(c)). Corresponding zoomed-in optical images show mechanical behaviors of the island-bridge structure under different tensile strain. For capacitive sensing, higher capacitance leads to lower input impedance,  $Z$

$$Z = \frac{1}{2\pi f c}$$

where  $f$  is frequency and  $c$  is capacitance. A lower input impedance will result in a higher signal amplitude, because

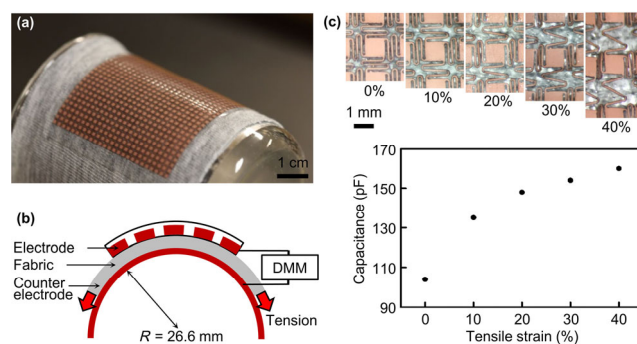


**Figure 3** Characterization of electrode capacitance under various tensile strain. (a) An optical image and (b) schematics of the measurement setup. DMM: digital multimeter. (c) Zoomed-in images of the electrode (top) and capacitance (bottom) at different tensile strain levels.

less voltage will be dropped across the capacitive electrode. In the meantime, the background noise, which mainly comes from the circuit, remains the same regardless of the input impedance as illustrated in Fig. S3 in the ESM. Hence, the SNR can be increased.

## 2.4 Biopotential measurements

Figure 4(a) shows the schematic mechanism of the capacitive sensor. Buffer amplifiers are used for impedance matching to decrease the overall large coupling impedance of the capacitive electrodes. Both electrodes have common-mode 60-Hz noise. An instrumentation amplifier bolsters the potential difference between the two electrodes and reduces the common-mode noise. The signal is then output to an external data acquisition system (Picoscope 5000), which digitizes the signal at a sampling rate of 2,000 Hz and records the data. The external data acquisition system includes a built-in band-pass filter to eliminate the high-frequency noise produced by the human body and a 60 Hz digital notching filter (in Matlab).

EMG and ECG are measured on the forearm and the chest, respectively. To validate the performance of the capacitive electrode, a commercial wet electrode was used at the same position with the same circuit for acquiring ECG and EMG signals. Figure 4(b) shows typical EMG signals measured during repeated holding and releasing of a grip dynamometer. The red and black curves represent results from the capacitive electrode and wet electrode, respectively. Figure 4(c) shows typical ECG signals measured. The P, Q, R, S, and T waves are

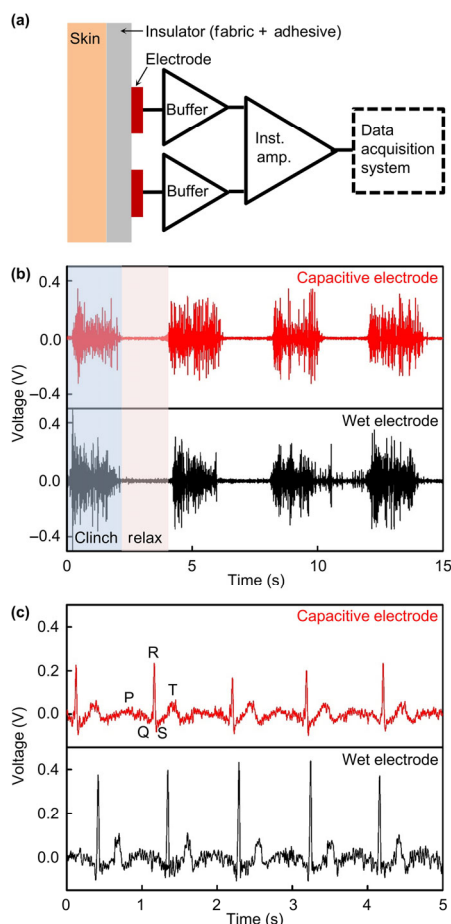


**Figure 4** Biopotential measurements with the stretchable capacitive sensor. (a) A schematic diagram of the capacitive sensor system. Signals are processed by buffer amplifiers and an instrumentation amplifier, and then transferred to a data acquisition system. (b) EMG and (c) ECG signals measured by the capacitive electrode and a commercial wet electrode. P, Q, R, S, T waves are labelled.

clearly defined. The output waveforms of these two electrodes show high correspondence to each other. It should be noted that to ensure the same testing location, these signals from the two different electrodes are collected one after another, resulting in slightly different waveforms.

## 2.5 Enhanced performance with CCTO-doped electrodes

To further enhance the SNR, we increased the dielectric constant of the adhesive layer by adding dielectric nanoparticles to form a composite (Fig. S4 in the ESM). Compared with niobate-lead titanate [30], barium titanate [31], and titanium dioxide [32], CCTO is lead-free, and has an ultra-high temperature-independent relative dielectric constant of more than  $10^4$  due to its unique structure [33, 34]. The average size of the CCTO particles is  $\sim 1 \mu\text{m}$  (Fig. 5(a)). We further characterized this particle with X-ray diffraction (XRD) and energy-dispersive X-ray spectroscopy (EDX), as shown in Fig. S4 in the ESM. With a 40 wt.% particle concentration and the thickness of the adhesive layer being the same, the electrode does not sacrifice its stretchability (Fig. 5(b) and Fig. S5 in the ESM; see the Experimental Section for detailed fabrication processes). The CCTO-composite electrode has a capacitance of 190 pF compared to 120 pF of the non-composite electrode. The reason for the finite improvement on capacitance is because when the adhesive layer capacitance is high, the fabric capacitance will become the bottleneck, as discussed in Fig. S6 in the ESM. We measured the ECG signal on the same subject (Fig. 5(c)). The overall signal amplitude is enhanced, and correspondingly, the SNR based on the R peak amplitude [35] is increased by 3 dB by the CCTO-composite.

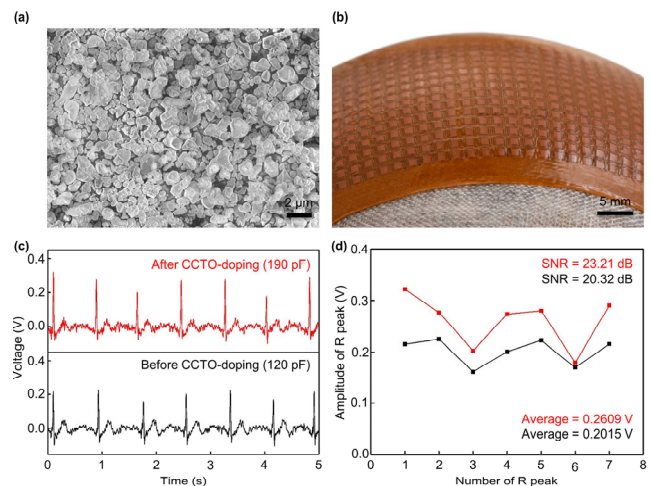


**Figure 5** Enhanced biopotential measurements by the CCTO-doped adhesive layer. (a) An SEM image of CCTO nanoparticles. (b) An optical image of the CCTO-doped electrode. (c) ECG signals measured using electrodes with and without CCTO on the same subject. (d) Corresponding signal amplitude, average amplitude, and SNR of the R-peaks.

## 3 Experimental section

A microscope glass slide was coated by poly(methyl methacrylate) (PMMA, 950 A4, MicroChem) as a release layer, and a 200  $\mu\text{m}$  thick layer of Ecoflex (Smooth-On). A separate microscope glass slide was coated with a 50  $\mu\text{m}$  thick polydimethylsiloxane (PDMS, 20:1, Sylgard 184 silicone elastomer), followed by laminating with a 20  $\mu\text{m}$  thick copper foil (Oak-Mitsui Inc.) [36]. The copper foil was then patterned by pulsed laser ablation (Precision Laser Processing system Model 01-14, Laser Mark's) according to the geometries designed in AutoCAD. After ultraviolet ozone activation for 3 min, a water-soluble tape (3M) was used to transfer the patterned copper filament to the

Ecoflex substrate. The water-soluble tape was then removed by soaking in water at 80 °C for 15 min. For electrodes of the device, an adhesion layer with thickness of ~ 200 μm (Silbione, RT Gel 4717 A/B, Bluestar Silicones) was spin-coated on the copper and cured at room temperature for 48 h. Also, CCTO powders (Stanford Advanced Material) were uniformly mixed with the silbione at 40 wt.%. The CCTO-doped silbione was spin-coated on the copper with a thickness of 200 μm. For bonding electronic components of the circuit, the transferred copper surface was cleaned using flux to improve wettability of the solder paste. Afterward, solder paste (SMDLTLFP, Chip Quik Inc.) was used to bond the integrated circuit components on the copper wire under an optical microscope by thermal reflow on a hotplate at 150 °C for 2 min. The electrodes and circuit were connected by solder paste. Ecoflex was coated and cured with a thickness of 200 μm as an encapsulation layer of the device. The electrodes and the circuit were transferred and bonded to the fabric by the adhesive layer.

#### 4 Conclusion

In this study, we demonstrated a wearable and stretchable non-contact biopotential sensing device on a fabric substrate. The electrodes exhibit high stretchability of over 100% that allows conformal contact with skin, and a large area ratio of over 70% that enables strong capacitive coupling with the skin. The electrodes and the circuit are integrated on a common substrate for signal acquisition and processing, with the resulting ECG and EMG signals comparable to commercial wet electrodes. Furthermore, we demonstrated that the device capacitance could be increased by compositing the adhesive layer with high dielectric constant CCTO nanoparticles, enhancing the SNR of the biopotential signals. These results offer a convenient way to measure ambulatory biopotential signals on clothing over the long term, which may greatly facilitate the adoption of wearable stretchable sensors.

#### Acknowledgement

We thank Yutaka Imai and Yota Komoriya for their support to this project and S. Xiang for constructive feedback on the manuscript preparation. This material is based on research sponsored by Air Force Research Laboratory under agreement number FA8650-18-2-5402. The U.S. Government is authorized to reproduce and distribute reprints for Government purposes notwithstanding any copyright notation thereon. The views and conclusions contained herein are those of the authors and should not be interpreted as necessarily representing the official policies or endorsements, either expressed or implied, of Air Force Research Laboratory (AFRL) or the U.S. Government. All bio-experiments were conducted with the approval of the Institutional Review Board of the University of California, San Diego.

**Electronic Supplementary Material:** Supplementary material (schematics of the circuit design and list of components, stretchability of different designs, and characterization of the CCTO particles) is available in the online version of this article at <https://doi.org/10.1007/s12274-021-3458-0>.

#### References

[1] Brugarolas, R.; Dieffenderfer, J.; Walker, K.; Wagner, A.; Sherman, B.; Roberts, D.; Bozkurt, A. Wearable wireless biophotonic and biopotential sensors for canine health monitoring. In *SENSORS, 2014 IEEE*, Valencia, Spain, 2014, pp 2203–2206.

[2] Samol, A.; Bischof, K.; Luani, B.; Pascut, D.; Wiemer, M.; Kaese, S. Single-lead ECG recordings including Einthoven and Wilson Leads by a smartwatch: A new era of patient directed early ECG differential diagnosis of cardiac diseases? *Sensors* **2019**, *19*, 4377.

[3] Ibaida, A.; Khalil, I. Wavelet-based ECG steganography for protecting patient confidential information in point-of-care systems. *IEEE Trans. Biomed. Eng.* **2013**, *60*, 3322–3330.

[4] Jeong, J. W.; Yeo, W. H.; Akhtar, A.; Norton, J. J.; Kwack, Y. J.; Li, S.; Jung, S. Y.; Su, Y. W.; Lee, W.; Xia, J. et al. Materials and optimized designs for human-machine interfaces via epidermal electronics. *Adv. Mater.* **2013**, *25*, 6839–6846.

[5] Dantas, H.; Warren, D. J.; Wendelken, S. M.; Davis, T. S.; Clark, G. A.; Mathews, V. J. Deep learning movement intent decoders trained with dataset aggregation for prosthetic limb control. *IEEE Trans. Biomed. Eng.* **2019**, *66*, 3192–3203.

[6] Dias, N. S.; Ferreira, J. F.; Figueiredo, C. P.; Correia, J. H. A wireless system for biopotential acquisition: An approach for non-invasive brain-computer interface. In *Proceedings of 2007 IEEE International Symposium on Industrial Electronics*, Vigo, Spain, 2007, pp 2709–2712.

[7] Lobodzinski, S. S.; Laks, M. M. New devices for very long-term ECG monitoring. *Cardiol. J.* **2012**, *19*, 210–214.

[8] Zehender, M.; Meinertz, T.; Keul, J.; Just, H. ECG variants and cardiac arrhythmias in athletes: Clinical relevance and prognostic importance. *Am. Heart J.* **1990**, *119*, 1378–1391.

[9] Gilgen-Ammann, R.; Schweizer, T.; Wyss, T. RR interval signal quality of a heart rate monitor and an ECG Holter at rest and during exercise. *Eur. J. Appl. Physiol.* **2019**, *119*, 1525–1532.

[10] Liu, S. H.; Lin, C. B.; Chen, Y.; Chen, W. X.; Huang, T. S.; Hsu, C. Y. An EMG patch for the real-time monitoring of muscle-fatigue conditions during exercise. *Sensors* **2019**, *19*, 3108.

[11] Li, G. L.; Wang, S. Z.; Duan, Y. Y. Towards conductive-gel-free electrodes: Understanding the wet electrode, semi-dry electrode and dry electrode-skin interface impedance using electrochemical impedance spectroscopy fitting. *Sens. Actuators B Chem.* **2018**, *277*, 250–260.

[12] Griffith, M. E.; Portnoy, W. M.; Stotts, L. J.; Day, J. L. Improved capacitive electrocardiogram electrodes for burn applications. *Med. Biol. Eng. Comput.* **1979**, *17*, 641–646.

[13] Spinelli, E.; Haberman, M.; García, P.; Guerrero, F. A capacitive electrode with fast recovery feature. *Physiol. Meas.* **2012**, *33*, 1277–1288.

[14] Sun, Y.; Yu, X. B. Capacitive biopotential measurement for electrophysiological signal acquisition: A review. *IEEE Sens. J.* **2016**, *16*, 2832–2853.

[15] Portelli, A. J.; Nasuto, S. J. Design and development of non-contact bio-potential electrodes for pervasive health monitoring applications. *Biosensors* **2017**, *7*, 2.

[16] Sundaram, P. S. S.; Basker, N. H.; Natrayan, L. Smart clothes with bio-sensors for ECG monitoring. *Int. J. Innov. Technol. Explor. Eng.* **2019**, *8*, 298–301.

[17] Pehr, S.; Zollitsch, D.; Güttler, J.; Bock, T. Development of a non-contact ECG application unobtrusively embedded into a bed. In *Proceedings of 2019 IEEE Sensors Applications Symposium (SAS)*, Sophia Antipolis, France, 2019, pp 1–6.

[18] Singh, R. K.; Sarkar, A.; Anoop, C. S. A health monitoring system using multiple non-contact ECG sensors for automotive drivers. In *Proceedings of 2016 IEEE International Instrumentation and Measurement Technology Conference Proceedings*, Taipei, China, 2016, pp 1–6.

[19] Das, P. S.; Park, J. Y. A flexible touch sensor based on conductive elastomer for biopotential monitoring applications. *Biomed. Signal Process. Control* **2017**, *33*, 72–82.

[20] Jeong, J. W.; Kim, M. K.; Cheng, H.; Yeo, W. H.; Huang, X.; Liu, Y. H.; Zhang, Y. H.; Huang, Y. G.; Rogers, J. A. Capacitive epidermal electronics for electrically safe, long-term electrophysiological measurements. *Adv. Healthc. Mater.* **2014**, *3*, 642–648.

[21] Dong, W. T.; Cheng, X.; Xiong, T.; Wang, X. M. Stretchable biopotential electrode with self-similar serpentine structure for continuous, long-term, stable ECG recordings. *Biomed. Microdevices* **2019**, *21*, 6.

[22] Das, P. S.; Kim, J. W.; Park, J. Y. Fashionable wrist band using

- highly conductive fabric for electrocardiogram signal monitoring. *J. Ind. Textiles* **2019**, *49*, 243–261.
- [23] Wang, H. M.; Wang, H. M.; Wang, Y. L.; Su, X. Y.; Wang, C. Y.; Zhang, M. C.; Jian, M. Q.; Xia, K. L.; Liang, X. P.; Lu, H. J. et al. Laser writing of janus graphene/kevlar textile for intelligent protective clothing. *ACS Nano* **2020**, *14*, 3219–3226.
- [24] Liang, X. P.; Li, H. F.; Dou, J. X.; Wang, Q.; He, W. Y.; Wang, C. Y.; Li, D. H.; Lin, J. M.; Zhang, Y. Y. Stable and biocompatible carbon nanotube ink mediated by silk protein for printed electronics. *Adv. Mater.* **2020**, *32*, 2000165.
- [25] Zhang, M. C.; Wang, C. Y.; Liang, X. P.; Yin, Z.; Xia, K. L.; Wang, H. M.; Jian, M. Q.; Zhang, Y. Y. Weft-knitted fabric for a highly stretchable and low-voltage wearable heater. *Adv. Electron. Mater.* **2017**, *3*, 1700193.
- [26] Yuan, L.; Zhang, M.; Zhao, T. T.; Li, T. K.; Zhang, H.; Chen, L. L.; Zhang, J. H. Flexible and breathable strain sensor with high performance based on MXene/nylon fabric network. *Sens. Actuators A Phys.* **2020**, *315*, 112192.
- [27] Gong, M.; Wan, P. B.; Ma, D.; Zhong, M. J.; Liao, M. H.; Ye, J. J.; Shi, R.; Zhang, L. Q. Flexible breathable nanomesh electronic devices for on-demand therapy. *Adv. Funct. Mater.* **2019**, *29*, 1902127.
- [28] Huang, Z. L.; Hao, Y. F.; Li, Y.; Hu, H. J.; Wang, C. H.; Nomoto, A.; Pan, T. S.; Gu, Y.; Chen, Y. M.; Zhang, T. J. Three-dimensional integrated stretchable electronics. *Nat. Electron.* **2018**, *1*, 473–480.
- [29] Jang, K. I.; Han, S. Y.; Xu, S.; Mathewson, K. E.; Zhang, Y. H.; Jeong, J. W.; Kim, G. T.; Webb, R. C.; Lee, J. W.; Dawidczyk, T. J. Rugged and breathable forms of stretchable electronics with adherent composite substrates for transcutaneous monitoring. *Nat. Commun.* **2014**, *5*, 4779.
- [30] Gallone, G.; Carpi, F.; De Rossi, D.; Levita, G.; Marchetti, A. Dielectric constant enhancement in a silicone elastomer filled with lead magnesium niobate–lead titanate. *Mater. Sci. Eng. C* **2007**, *27*, 110–116.
- [31] Bele, A.; Stiubianu, G.; Varganici, C. D.; Ignat, M.; Cazacu, M. Silicone dielectric elastomers based on radical crosslinked high molecular weight polydimethylsiloxane co-filled with silica and barium titanate. *J. Mater. Sci.* **2015**, *50*, 6822–6832.
- [32] Cherney, E. A. Silicone rubber dielectrics modified by inorganic fillers for outdoor high voltage insulation applications. *IEEE Trans. Dielectrics Electrical Insulat.* **2005**, *12*, 1108–1115.
- [33] Singh, D. P.; Mohapatra, Y. N.; Agrawal, D. C. Dielectric and leakage current properties of sol–gel derived calcium copper titanate (CCTO) thin films and CCTO/ZrO<sub>2</sub> multilayers. *Mater. Sci. Eng. B* **2009**, *157*, 58–65.
- [34] Duan, L.; Wang, G. L.; Zhang, Y. Y.; Zhang, Y. N.; Wei, Y. Y.; Wang, Z. F.; Zhang, M. High dielectric and actuated properties of silicone dielectric elastomers filled with magnesium-doped calcium copper titanate particles. *Polym. Compos.* **2018**, *39*, 691–697.
- [35] Vlach, K.; Kijonka, J.; Jurek, F.; Vavra, P.; Zonca, P. Capacitive biopotential electrode with a ceramic dielectric layer. *Sens. Actuators B Chem.* **2017**, *245*, 988–995.
- [36] Yang, Y.; Hu, H. J.; Chen, Z. Y.; Wang, Z. Y.; Jiang, L. M.; Lu, G. X.; Li, X. J.; Chen, R. M.; Jin, J.; Kang, H. C. et al. Stretchable nanolayered thermoelectric energy harvester on complex and dynamic surfaces. *Nano Lett.* **2020**, *20*, 4445–4453.